Hindawi
Geofluids
Volume 2022, Article ID 8270471, 13 pages
https://doi.org/10.1155/2022/8270471

Research Article

Experimental Study on Axial Compression Performance of 7A04 High Strength Aluminum Alloy Circular Tube Concrete Short Column

Zuo-Jin Zhang,[1] **Feng-Xia Han**,[1,2] **and Qing Liu**[1,2]

[1]*School of Civil Engineering and Architecture, Xinjiang University, Urumqi 830047, China*
[2]*Xin Jiang Key Lab of Building Structure and Earthquake Resistance, China*

Correspondence should be addressed to Feng-Xia Han; fxhan@xju.edu.cn

Received 21 January 2022; Revised 28 February 2022; Accepted 4 March 2022; Published 29 March 2022

Academic Editor: Wen-long Shen

The application of tube-filled concrete composite columns is becoming more and more popular. The traditional tube-filled column is easy to rust and expensive to maintain, which leads to the practical need of replacing high-strength aluminum alloy. 7A04 aluminum alloy has high strength and strong corrosion resistance, which is more in line with the material requirements of modern building structures. In view of this, four groups of 7A04 aluminum alloy tube concrete short columns were tested under axial compression, and the corresponding ABAQUS finite element simulation was established. The influence of tube thickness and concrete strength grade on compressive strength, ductility, transverse deformation coefficient, and improvement coefficient of strong concrete strength of composite column is considered in this paper. The results show that the failure mode of composite short columns is central uplift or shear failure. The tube thickness of high-strength aluminum tube has a great influence on the strength of specimens, and the ductility of composite columns decreases with the decrease of the collar coefficient. The finite element model can well reflect the development trend of the load-strain curve, and the formula of composite column bearing capacity proposed by regression analysis can well predict the strength of 7A04 aluminum alloy tubular concrete short column. The research results have a certain reference significance for the structural design of high strength aluminum concrete-filled columns.

1. Introduction

Concrete-filled steel tubular (CFST) columns are widely used in various composite structures with superior performance in terms of strength, ductility, and seismic resistance [1–3]. In-depth studies on CFST specimens have been conducted by many civil engineering designers and scholars [4, 5], the history and development of CFST in engineering application are summarized, and the application of CFST in various scenarios is discussed [6, 7]. However, the poor corrosion resistance of CFST restricts its application in various extreme conditions. CFST structures are not only expensive to maintain but also prone to various economic losses and even catastrophic events due to corrosion of steel tubes [8, 9]. The simple antirust treatment of CFST cannot meet its long-term use requirements of it.

Aluminum alloy is favored by the majority of civil engineering designers for its characteristics of light weight, high strength, high corrosion resistance, good processing performance, and easy regeneration as utilized in the Beijing Daxing International Airport (China), Staples Center (America), Leadenhall Tower (Britain), and Japan Tokyo Dome sports center (Japan). At present, aluminum alloy structure has been widely used in civil engineering, such as bridges, houses, and aluminum alloy roofs [10–12]. In order to fully explore the material properties of aluminum alloys, the literature [13, 14] carried out a detailed study of aluminum alloys, the results show that similar to structural steel, the aluminum alloy has remarkable ductility and is easier to extrude stronger corrosion resistance than steel, and there is almost no need for anticorrosion treatment in the later stage. Although the development of aluminum alloy

structure is limited by its high price and special welding process, however, with the promulgation of China's first Code for "CODE for DESIGN of ALUMINIUM STRUCTURES" [15], the research and application of aluminum alloy structures have entered a stage of rapid development now.

Zeng et al. [16, 17] explored the mechanical performance and failure behaviors of the aluminum alloy tube concrete short column by strengthening the two ends of the aluminum alloy tube. The results show that the aluminum alloy surface bulges when the short column fails, and the filled concrete is mostly oblique cross-section. With the increase of the strength of the filled concrete, the overall ductility of the composite column decreases. Feng et al. [18] has extensively studied the influence of section size and material properties on concrete filling in aluminum alloy tubes, which has been verified by experiments while conducting finite element design and research. The results show that the American and New Zealand codes do not consider the conformity between the aluminum tube and the concrete, and the calculation results are relatively conservative. Wang et al. [19] carried out a series of parametric studies on aluminum-tube concrete by comparing the experimental results with the finite element results and verified the adaptability of the calculation method of concrete-filled steel tubular column to the calculation method of aluminum-tube concrete. Lu et al. [20] and Feng et al. [21] have studied the static properties of aluminum-tube concrete bending specimens. It was shown that aluminum-tube concrete specimens also have good bending properties. Chen et al. [22] carried out in-plane bending tests on concrete-filled aluminum alloy thin-walled tubes. The ultimate strength, failure mode, flexural stiffness, ductility, and curve of specimens were studied to find out that the initial flexural stiffness, and postyield flexural stiffness of the CFAT specimens generally decreased by reinforcing with the CFRP.

The 7 series aluminum alloy has higher strength and better ductility than ordinary aluminum alloy. The use of 7series aluminum alloy instead of ordinary aluminum alloy can reduce the section area of the specimen and reduce the weight of the structure, which is more in line with the material requirements of high-rise buildings and large-span structures. Most of the researches focus on 5 series and 6 series aluminum alloy at present, and the researches on 7 series aluminum alloy are relatively few and mostly focus on the material itself, which limits its application in practical engineering. 7A04 aluminum alloy has high strength, but poor plasticity index [23, 24]; and its elastic modulus is only one third of that of steel. The high corrosion resistance of 7A04 aluminum alloy can avoid rusting during use [25]. Therefore, it is necessary to conduct further research on 7 series aluminum alloy filled concrete specimens. In this paper, four groups of 7A04 aluminum tube concrete short columns were tested and analyzed by the finite element method. The influence of tube thickness of aluminum tube and concrete material strength on the mechanical properties of aluminum tube concrete was explored. Finally, the ratio of the sectional composite compressive strength to the axial compressive strength of concrete and the collar coefficient was analyzed, and the bearing capacity calculation formula of 7A04 aluminum alloy tubular concrete short column was proposed based on the test results and finite element simulation.

2. Experimental Program

2.1. Material Properties. The PO42.5R ordinary Portland cement was supplied by Urumqi Tianshan Cement Factory in Xinjiang China, the fly-ash is local grade II, and the aluminum alloy tube (7A04) is produced by Gaosheng Aluminum Industry Co., Ltd., (Guangdong, China). Both ends of the specimen are not sealed and the specimen curing for 28 d after the completion of pouring.

This paper is based on the design of specimen size in reference [26–30], and four group specimens were used to test the strength characteristics of aluminum alloy circular tube concrete, as shown in Figure 1. The basic parameters of specimen design are shown in Table 1, and the concrete compressive strength test result and mechanical properties of aluminum alloy material are shown in Tables 2 and 3, respectively.

2.2. Column Testing Procedure. The specimen loading device is shown in Figure 2. The axial compression test was carried out on a hydraulic servo press controlled by YJW10000 microcomputer from the Key Laboratory of Seismic Resistance of Xinjiang University, which loading range of 5000 kN. And the loading system was determined according to GB/T 50152-2012 "STANDARD for TEST METHODS of CONCRETE STRUCTURES," and displacement control loading was adopted with a loading rate of 2 mm/min. When the vertical displacement of the specimen exceeds 60 mm, the load is stopped, and the specimen is considered to be damaged.

The vertical displacement of the specimen, the transverse, and longitudinal strain of the aluminum tube were measured continuously during the loading process. The displacement meter is placed parallel to the specimen along the height to measure the overall vertical displacement and verify the concentricity of the axial load at the initial loading stage (Figure 2). A displacement meter is also set to measure the horizontal displacement of the specimen in the meantime and the horizontal expansion of concrete under compression conditions. The strain gauge is arranged as shown in Figure 3. Measuring points are arranged at the upper, middle, and lower heights of the specimens, respectively, to measure the transverse and vertical strains of concrete. The top of the specimen is rigidly constrained with the testing machine, and the bottom is free in the horizontal direction without additional torque, and only vertical load exists in the whole process.

3. Results and Analysis

3.1. Load-Displacement Curves. Figure 4 shows the typical axial load-strain relationship, and the axial load-strain relationship is shown in Figure 5. The curve in Figure 4 has four points, which can be divided into four stages according to different stiffness: (1) *O-A* is the elastic stage, (2) *A-B* is the elastoplastic stage, (3). *B-C* is the plastic stage, and (4)

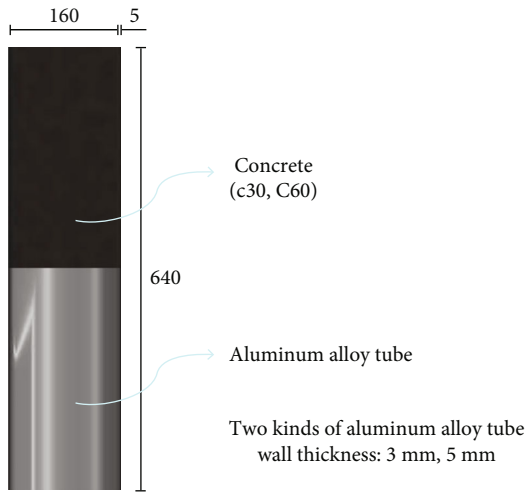

Figure 1: Specimen parameter diagram.

Table 1: Basic parameter table of specimen design.

Specimen label	Diameter D (mm)	Thickness t (mm)	Length L (mm)	f_{cu} (MPa)
ACST3	160	3	640	35.8
ACST5	160	5	640	35.8
AHCST3	160	3	640	67.6
AHCST5	160	5	640	67.6

*In "ACST (X)," "ACS" refers to the ordinary concrete column of aluminum alloy pipe, and "$T(x)$" refers to the tube thickness of the pipe. *In "AHCST (X)," "AHCS" is the high-strength concrete column of aluminum alloy tube, and "$T(x)$" is the tube thickness of the tube. f_{cu} is the compressive strength of the concrete.

Table 2: Concrete compressive strength test results.

Specimen label	Cubic compressive strength (MPa)	Average value (MPa)	Poisson's ratio υ
C30-1	33.7		0.23
C30-2	34.2	35.8	0.23
C30-3	39.6		0.23
C60-1	71.2		0.23
C60-2	63.6	67.6	0.23
C60-3	68.1		0.23

Table 3: Mechanical properties of aluminum alloy material.

Thickness	$f_{0.2}$ (MPa)	Tensile strength (MPa)	Poisson's ratio υ	Elasticity modulus E (MPa)
3	400	470	0.3	71000
5	450	550	0.3	71000

*$f_{0.2}$ is the yield strength of aluminum alloy.

C-D is the strain softening stage. C, the peak point of the curve, indicates that the whole specimen cross-section is in the plastic state and the confinement of concrete reaches the maximum value. The strength of specimens begins to decrease at a constant rate after point C. This can be explained by the strength gain from the aluminum tubes being less than the strength loss caused by concrete failure in the plastic stage. The variation trend of specimens in elastic and elastic-plastic stages is basically consistent with that of ordinary CFST specimens. The variation trend of curves in plastic and strain softening stages is different from that of CFST specimens.

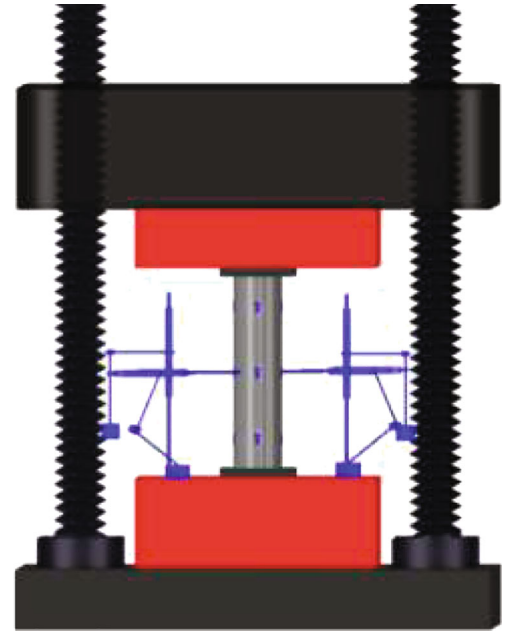

Figure 2: Specimen loading device.

The curve shows a linear relationship between load and displacement and keeps a higher slope rising. The decrease of the slope of the curve indicates that the stiffness of specimens decreases in elastic-plastic stage. The plastic development stage of all specimens is short because the aluminum tube has yielded at this time, and the core concrete has exceeded the compressive strength. However, the concrete is crushed to squeeze the aluminum tube, and the aluminum tube provides limited lateral constraints on the core concrete, which leads to the short plastic stage. When the load of the specimen passed the peak point and the specimen entered the softening stage, the curve continued to decrease. At this time, the aluminum tube followed the change of von-Mises yield ellipse trajectory, and the vertical pressure was gradually reduced, but the lateral constraint stress provided to the concrete along the radial direction was also limited. Concrete strength begins to decline due to concrete degradation. The load on the specimen decreases continuously until the specimen is destroyed. Due to the thin tube wall of the 3 mm specimen, the surface of the aluminum alloy is easy to crack as the load continues to increase after the peak point. At this time, the aluminum alloy can no longer bear the load, resulting in a sharp drop in the load of the specimen.

As can be seen from Figure 5, the curve decreases slowly when the tube thickness of the aluminum tube is 5 mm. The strength and ductility of the specimen with a tube thickness

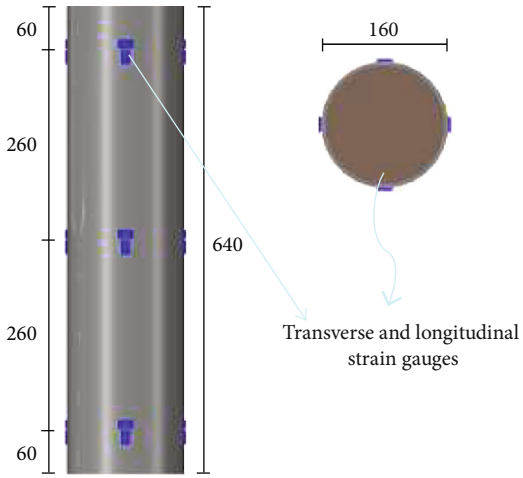

Figure 3: Position of strain gauge.

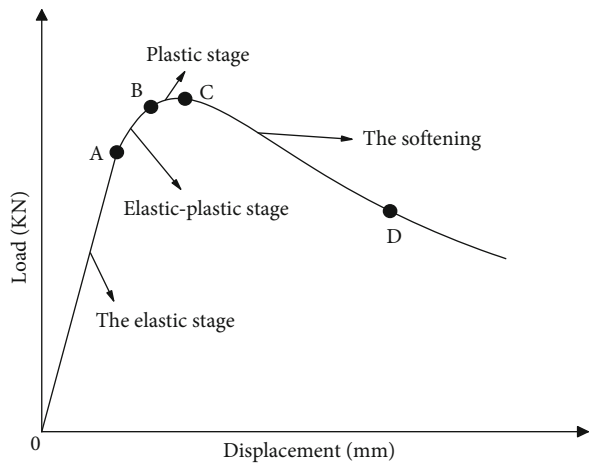

Figure 4: Typical load-displacement curves.

of 5 mm are slightly higher than those with a tube thickness of 3 mm. In order to obtain reasonable working performance of the specimen, increasing the tube thickness of the specimen and filling in ordinary concrete working together to meet the needs of practical engineering preferably.

The test bearing capacity is shown in Tables 4 and 5 below. The bearing capacity of specimens can be increased significantly when increasing concrete strength and tube thickness of the aluminum tubes. The increase of tube thickness improves the strength of the specimen among them especially. For the aluminum tube specimen filled with ordinary concrete, the ultimate bearing capacity of the specimen can be increased by 28% with the increase of tube thickness. The ultimate bearing capacity of high-strength concrete specimen can be increased by 24% with the increase of tube thickness. When the tube thickness is 3 mm and 5 mm, respectively, with the concrete strength grade being increased from C30 to C60, the ultimate bearing capacity of specimens is only increased by 8% and 5%. Therefore, increasing the tubes thickness of aluminum tube can better meet the need of bearing capacity of specimens in engineering.

3.2. Coefficient of Lateral Deformation. The coefficient of lateral deformation is the absolute value of the ratio of horizontal strain to a longitudinal strain of the specimen (Poisson's ratio). The vertical strain and transverse expansion occur during the loading of the specimen. The vertical and transverse strain of aluminum tube can be measured by the strain gauge pasted on the surface of the specimen.

The surface strain of the aluminum alloy can reflect not only the bending deformation of specimen but also the restraint mechanism of aluminum alloy on concrete. Poisson's ratio can be expressed by the absolute value of the ratio of horizontal strain to vertical strain (Figure 6), where N is the load on the specimen, and N_u is the peak load on the specimen. The ordinate is the load of the specimen; the abscissa is the change of Poisson's ratio during the loading process on the surface of the aluminum tube.

Poisson's ratio of aluminum tube is about 0.3 in the elastic stage, and the elastic stage is the ascending stage with a large slope as shown in Figure 6; Poisson's ratio of concrete is about 0.2 at this time. The core concrete is not restricted by aluminum tube, because the deformation of aluminum tube and concrete is no longer consistent, resulting in the joint force of concrete and aluminum tube no longer exist. The specimen enters the elastic-plastic stage when the load increases to about $0.75N_u$ continuously, with Poisson's ratio of aluminum tube increasing gradually. The aluminum tube has produced a tightening force on concrete at this time, and the constraint on concrete reaches the maximum at the peak point. After the peak load point, aluminum alloy has yielded, the circumferential strain has exceeded the yield strain, and concrete cannot be restrained. Core concrete keeps squeezing tube wall with the increase of load, and the circumferential strain of aluminum tube increases rapidly. It is important to note that Poisson's ratio of specimens of aluminum alloy develops rapidly after entering the elastic-plastic phase. It shows that the ductility of 7 series aluminum alloy decreases while its strength increases at the same time compared with ordinary aluminum alloy. Due to the yield and large deformation of aluminum alloy, the constraint and strength degradation of concrete are reduced, and the development of specimen in plastic stage is restricted. This is different from steel's constraint on concrete.

3.3. Ductility Index. Ductility refers to the ability of a specimen to undergo large deformation without strength degradation. The axial ductility index is used to evaluate the ductility of aluminum-tube concrete components under axial compression. Tao et al. [26] proposed the definition of ductility index (DI) as follows:

$$\mathrm{DI} = \frac{\varepsilon_{85\%}}{\varepsilon_y}, \tag{1}$$

where $\varepsilon_{85\%}$ is the axial strain when the load drops to 85% of the ultimate load, $\varepsilon_y = \varepsilon_{75\%}/0.75$, $\varepsilon_{75\%}$ is the axial strain when the load in the prepeak stage reaches 75% of the ultimate load, and the calculation results are shown in Table 6. The ductility index of the specimens in this test is between 2.59 and 4.58. The ductility of the specimens increases with the

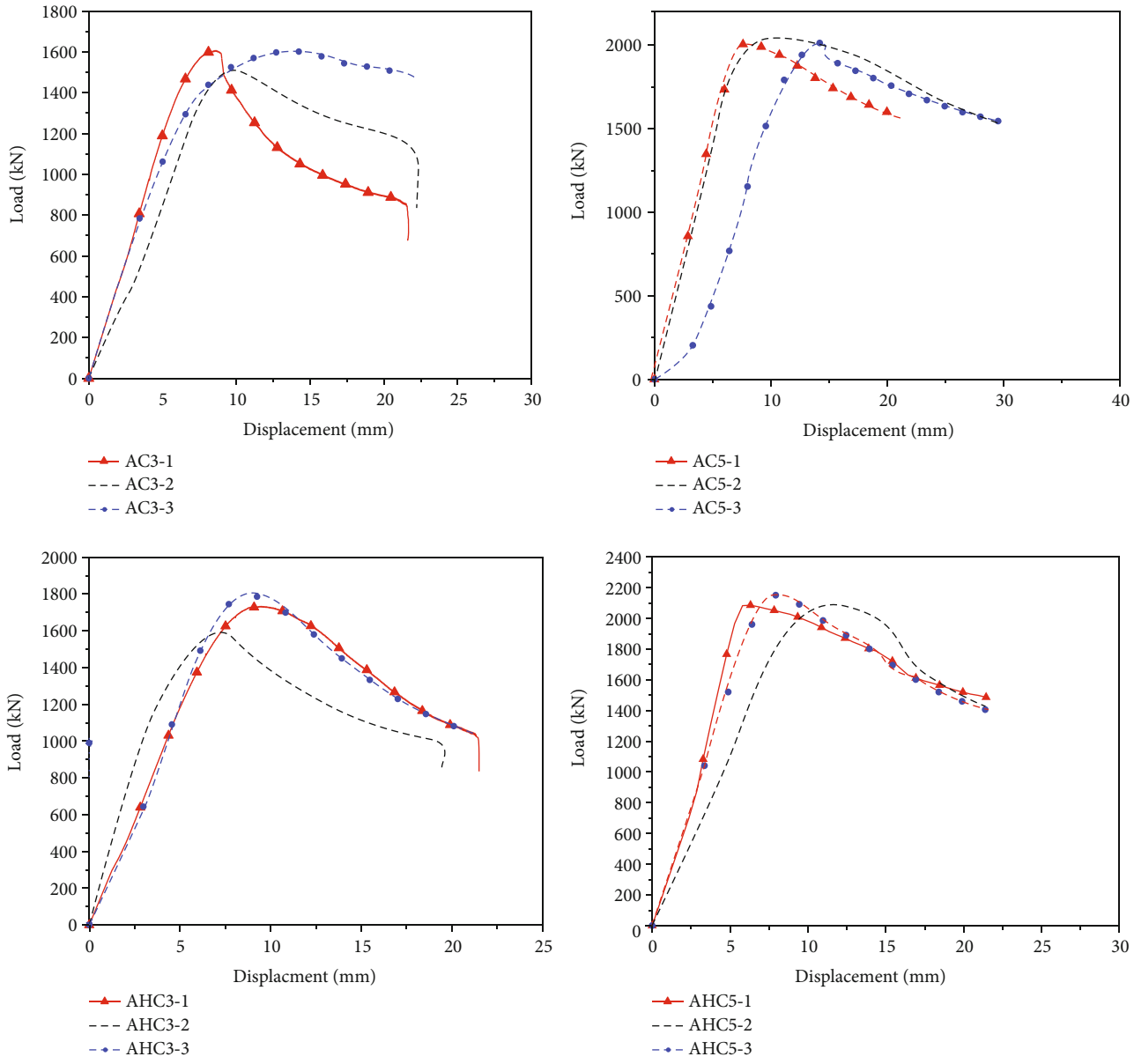

Figure 5: Test load-displacement curve.

Table 4: Axial compression test data.

Specimen label	Failure mode	N_u (kN)	(kN)
AC3-1	Swelling failure	1606.84	
AC3-2	Shear failure	1533.76	1581.57
AC3-3	Shear failure	1604.10	
AC5-1	Swelling failure $\bar{N}$	2010.74	
AC5-2	Swelling failure	2041.95	2022.09
AC5-3	Shear failure	2013.58	

*N_u is the ultimate bearing capacity, and $\bar{N}$ is the average bearing capacity of the specimen.

increase of the confinement coefficient, and the tube thickness of aluminum tube has a greater influence on the ductility of the specimens.

3.4. Constraints of Aluminum Tubes on Concrete. It can be seen from Table 6 that the ratio of ultimate strength to yield strength of aluminum tube is between 1.17 and 1.22. The strength of aluminum tubes is generally slightly lower than the yield strength under axial compression due to the presence of defects and circumferential stresses. The improvement of concrete strength and ductility is realized by the constraint of aluminum tube. By comparing the concrete bearing capacity with that of the plain concrete column, the constraint of aluminum tube on concrete can be estimated and analyzed roughly.

Because the load on the specimens is common to aluminum tube and concrete, the vertical load on the specimens cannot be measured directly. Therefore, the stress of the core concrete can be subtracted from the total load of the specimen by the force of the aluminum tube. And the force of

Table 5: Axial compression test data.

Specimen Labe	Failure mode	N_u (kN)	$\bar{N}$(kN)
AHC3-1	Swelling failure	1732.46	
AHC3-2	Shear failure	1594.08	1707.75
AHC3-3	Swelling failure	1796.70	
AHC5-1	Shear failure	2088.30	
AHC5-2	Swelling failure	2092.06	2110.70
AHC5-3	Swelling failure	2151.74	

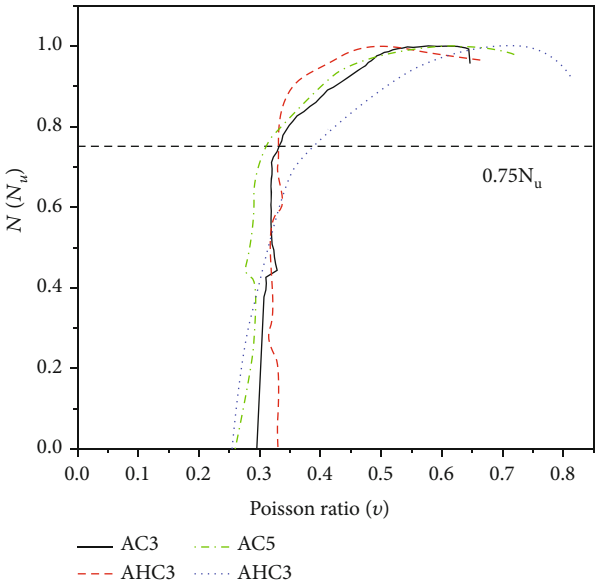

Figure 6: Poisson ratio.

Table 6: Ductility index and coefficient of strength improvement.

Specimen label	Confinement coefficient θ	Ductility index DI	Coefficient of strength improvement k
ACST3	1.31	3.23	1.63
ACST5	2.28	4.58	1.79
AHCST3	0.735	2.59	1.09
AHCST5	1.27	4.03	1.49

*$f_{0.2}$ is the yield strength of aluminum alloy, $\theta = f_{0.2}A_A/f_{ck}A_C$ is the confinement coefficient, $f_{0.2}$ is the yield strength of aluminum tube, f_{ck} is the axial compressive strength of concrete, A_A is the sectional area of aluminum tube, and A_c is the axial compressive strength of concrete, sectional area of concrete.

the aluminum tube can be multiplied by the measured yield strength of the aluminum tube by the cross-section area of it, when the specimen bears the peak load. The constraint of the aluminum tube on inner core concrete can be roughly predicted and analyzed according to the calculated load of concrete. The compressive strength f_c' of concrete can be obtained by dividing the load borne by the cross-section area of concrete. The coefficient of strength improvement of concrete constrained by aluminum tube can be obtained by dividing the f_c' by axial compressive strength of concrete f_c, which is expressed by k value. The calculation results are shown in Table 6 and Figure 7. In Figure 7, D/t is the ratio of diameter to thickness.

The coefficient of strength improvement of concrete is 1.78 while the confinement coefficient is 0.735. The coefficient of strength improvement of concrete is only 1.09 when the confinement coefficient is 2.38. The coefficient of strength improvement decreases gradually with the increase of confinement coefficient. The diameter to thickness ratio has a greater influence on k value among them. This is because for high-strength aluminum alloy, the greater the tube thickness of the specimen with the same cross-section, the stronger the constraint on the side confining pressure of concrete, which can better resist the transverse expansion of concrete and limit the generation and expansion of cracks in concrete. With the improvement of concrete strength grade, the constraint of the aluminum tubes on core concrete gradually decreases. This may be because the greater the compressive strength of concrete, the greater the pressure borne by concrete when the proportion of axial force borne by concrete and aluminum tube changes constantly in the elastic-plastic stage. The higher the strength of concrete, the worse the plasticity, when concrete is crushed under too much pressure, internal cracks gradually increase, and concrete transverse expansion causes the aluminum alloy to swell and spring. The lateral confining pressure of aluminum tube wall on concrete is limited if the section diameter to thickness ratio is too large, which the transverse expansion of concrete cannot be well restricted, and then the swelling deformation is further increased; the constraint of aluminum alloy on concrete is very limited at this time. Therefore, the interaction between aluminum tube and concrete can be fully utilized if ordinary concrete is filled in the specimen with a small to thickness ratio to maximize its utilization while satisfying the sufficient ductility of the specimen.

3.5. Failure Modes and Characteristics. The failure modes of the specimens are basically the same, and they are finally presented as the central swelling failure or shear failure, as shown in Figures 8(a) and 8(b). Due to the low ductility of 7 series aluminum alloy, it fails to produce good plastic deformation like steel tube after yielding, and the increasing load leads to aluminum alloy tube cracking in the meanwhile, as shown in Figure 8(c).

When the specimen is subjected to a larger load, the aluminum alloy begins to yield while the concrete expands horizontally, leading to swelling in the middle of the specimen. The stress on the swelling position of aluminum alloy is small, which weakens the constraint of aluminum alloy on concrete. The concrete at the swelling position is less constrained, the vertical pressure borne by concrete increases continuously with the increase of external load, and the concrete at the swelling position further expands, resulting in the final failure of the specimen.

Due to the self-weight of concrete and the vibration process, the coarse aggregate is easy to flow to the bottom, and the concrete at the end is fragile. Another reason is the uneven concrete at the end of the specimen did not fully

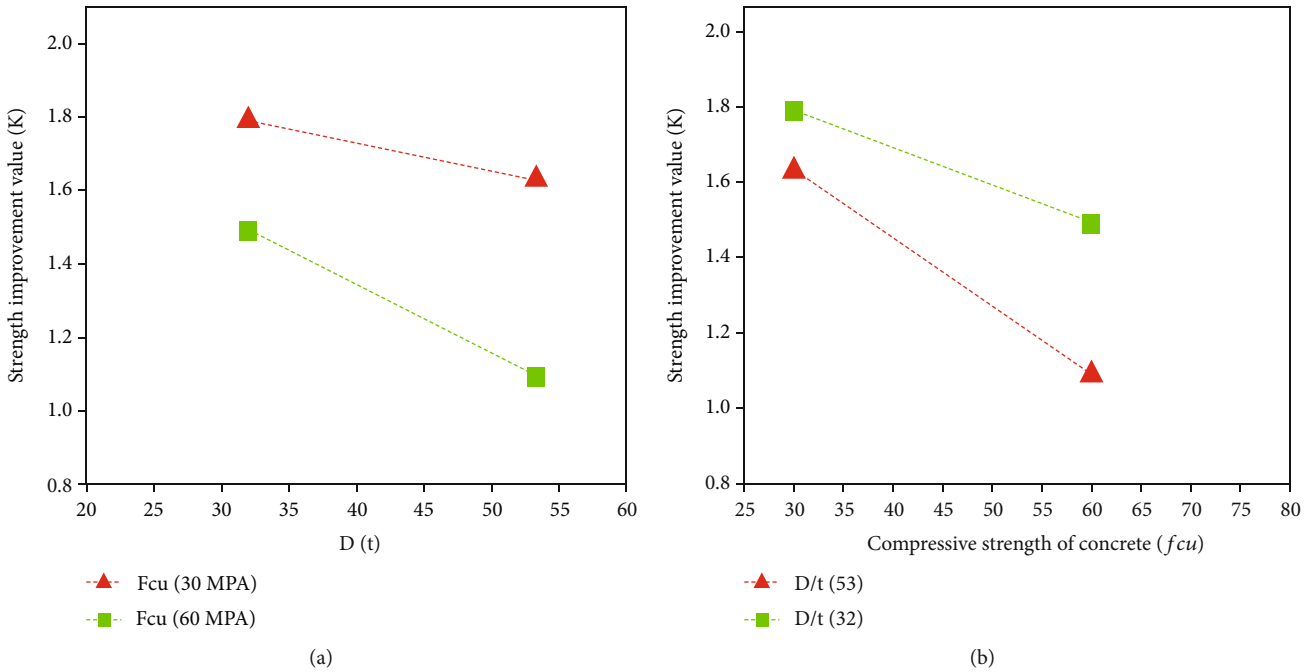

Figure 7: Concrete strength improvement value.

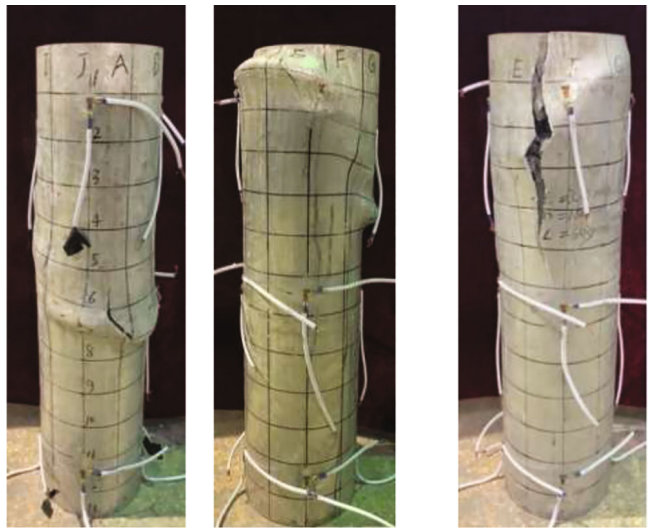

Figure 8: Failure pattern of aluminum alloy concrete columns.

contact with the cover plate, and the existence of the end effect in the loading process made the end of the aluminum tube bear a large force; the concrete drives the aluminum tube to produce oblique slip. The deformation further increased as the load continued to increase, resulting in shear failure.

Microcracks and damage emerge in the internal of concrete in the initial stage of loading, aluminum alloy tube which limits the development of the internal micro cracks. The proportion of axial force between the aluminum alloy tube and the concrete changes with the displacement of continuous loading. The concrete inside begins to swell and the cracks grow, resulting in macroscopic deformation. Outward swelling cracking of the aluminum tube occurred because the inward buckling is limited by the concrete.

Due to the low aluminum content of the specimen cross-section, the 3 mm specimen has limited constraints on concrete. Before the load of the specimen reaches the peak point, the concrete expands horizontally and squeezes the tube wall continuously, causing slight swelling in the middle or upper part of the specimen. As the load continues to increase, the constraint effect of aluminum alloy tube is limited, resulting in small cracks on the surface of aluminum alloy tube, and easy to crack in weak position.

For 5 mm specimens, the surface of aluminum alloy changes a little before the peak point, and the swelling

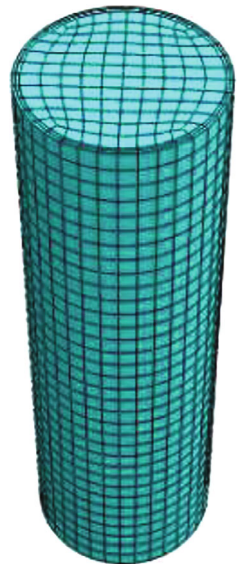

Figure 9: Finite element model.

deformation of aluminum alloy occurs after the curve reaches the peak point. The aluminum tube has a stronger constraint on concrete due to the large content of aluminum in the cross-section of the specimen, which effectively inhibits the horizontal expansion of concrete, and the small cracks on the surface of aluminum alloy are relatively less.

The strength grade of concrete has little influence on the test phenomenon in the process of this test. The failure modes of the test concrete are the fracture of weak aggregate and mortar, and the separation of mortar and coarse aggregate. The specimen filled with high-strength concrete is easier to crush, and the cracking degree of the aluminum tube is relatively larger compared with the specimen filled with ordinary concrete for the one with a tube thickness of 3 mm. The failure modes of filled ordinary concrete and filled high strength concrete are relatively uniform for specimens with 5 mm tube thickness.

4. Finite Element Simulation of a Composite Column

Aluminum tubes are filled with concrete, and the two of them are interactive. On the one hand, the transverse expansion and crack development of concrete filler can be limited by aluminum tubes; on the other hand, concrete also restricts the inward bending of aluminum tube. In order to represent the interaction between aluminum tube and concrete correctly, it is very important to select an appropriate constitutive model during simulation.

4.1. Constitutive Model of Aluminum Alloy. Ramberg-Osgood's model can better reflect the actual properties of aluminum alloy; so, this model has been widely used [31]. The constitutive model is expressed as follows:

$$\varepsilon = \frac{\sigma}{E} + \left(\frac{\sigma}{B}\right)^n, \tag{2}$$

Figure 10: Nephogram of finite element calculation.

where E is the initial elastic modulus of origin, and B and n can be measured by the test.

When the residual strain is equal to 0.002, the corresponding stress is the yield strength $f_{0.2}$ that can be obtained from Equation (2).

$$0.002 = \varepsilon - \frac{f_{0.2}}{E} = \left(\frac{f_{0.2}}{B}\right)^n. \tag{3}$$

Substitute Equation (3) into equation (2).

$$\varepsilon = \frac{\sigma}{E} + 0.002\left(\frac{\sigma}{f_{0.2}}\right)^n. \tag{4}$$

The index n is a parameter to describe strain hardening. To facilitate calculation, SteinHard [32] proposed an approximate calculation formula in 1971. The expression is as follows:

$$10n = f_{0.2}. \tag{5}$$

4.2. Constitutive Model of Concrete. The improvement of the strength and ductility of aluminum alloy tubes on concrete is fully considered. The classical Minder model is adopted to calculate based on the study of Ishvarbhai et al. [33–34]. After repeated simulation, a constitutive model more

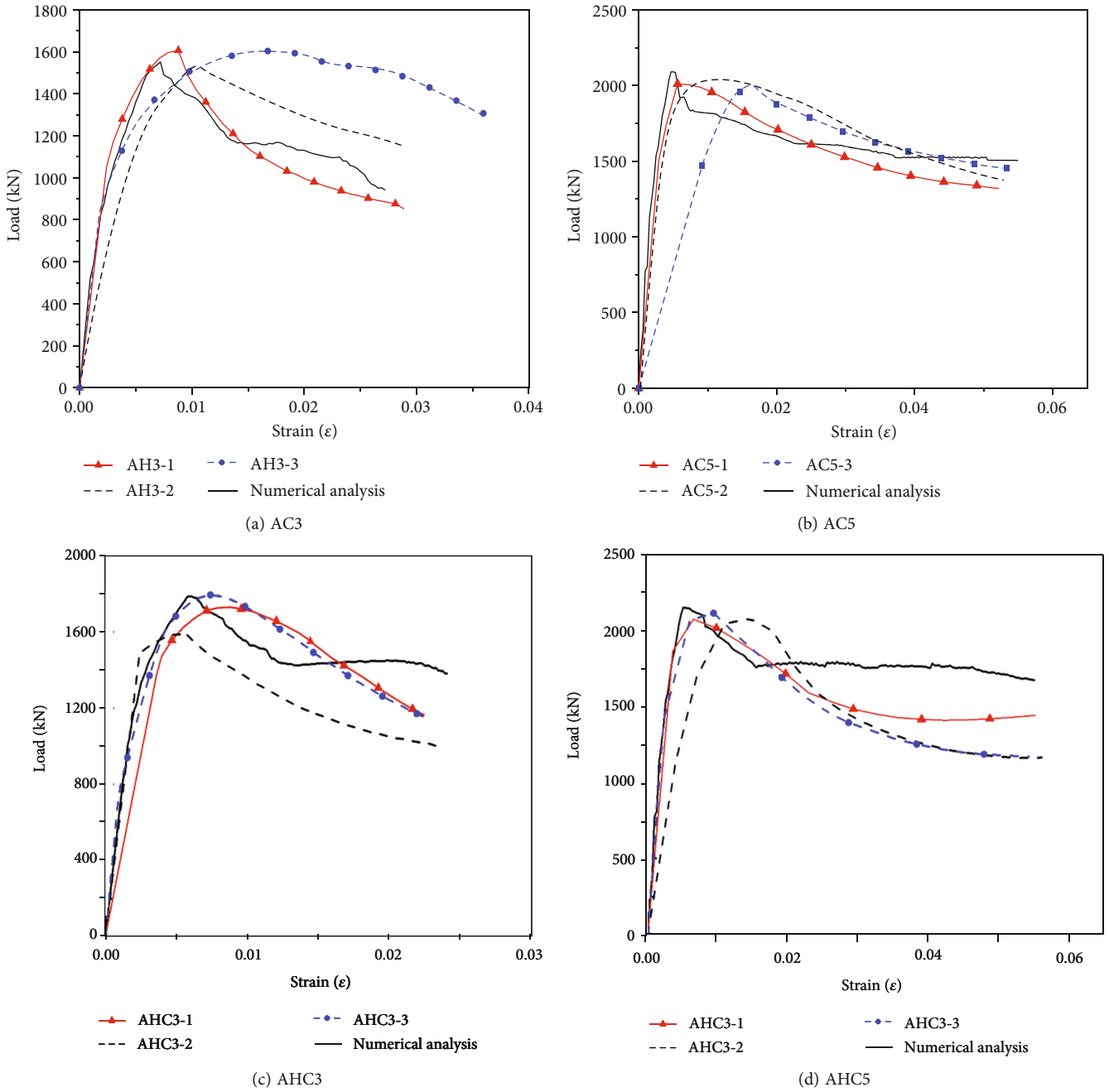

Figure 11: Comparison of experimental and finite element results.

suitable for 7A04 aluminum alloy tube concrete column is proposed as follows:

$$\sigma = \frac{f_{cc} x r}{r - 1 + x^r}, \tag{6}$$

$$x = \frac{\varepsilon}{\varepsilon_{cc}}, \quad r = \frac{E_C}{E_{\text{sec}} - E_{\text{sec}}}. \tag{7}$$

When $x \le 1$, $f_{cc} = \gamma_c f_c' + k_1 f_{rp}$, $x > 1$, and $f_{cc} = 0.79 f_{cu}$.

$$\gamma_c = 1.85 D_c^{-0.135} \ (0.85 \le \gamma_c \le 1.0), \tag{8}$$

$$f_{rp} = \left(0.006241 - 0.0000357 \frac{D}{t}\right) f_y. \tag{9}$$

E_c is the elastic modulus of concrete, $E_c = 4730 \times \sqrt{f_c}$; E_{sec} is the peak stress secant stiffness, $E_{\text{sec}} = f_{cc}/\varepsilon_{cc}$; $k_1 = 4.1$, $k_2 = 20.5$; and ε_{cc} is the peak strain.

Table 7: Comparison between test results and finite element calculation.

Specimen label	Test results N (kN)	Finite element calculation N_f (kN)	N/N_f
ACST3	1581	1551	1.019
ACST5	2022	2090	0.967
AHCST3	1707	1787	0.956
AHCST5	2110	2148	0.983

*N is the test peak bearing capacity; N_f is finite element calculation of peak bearing capacity.

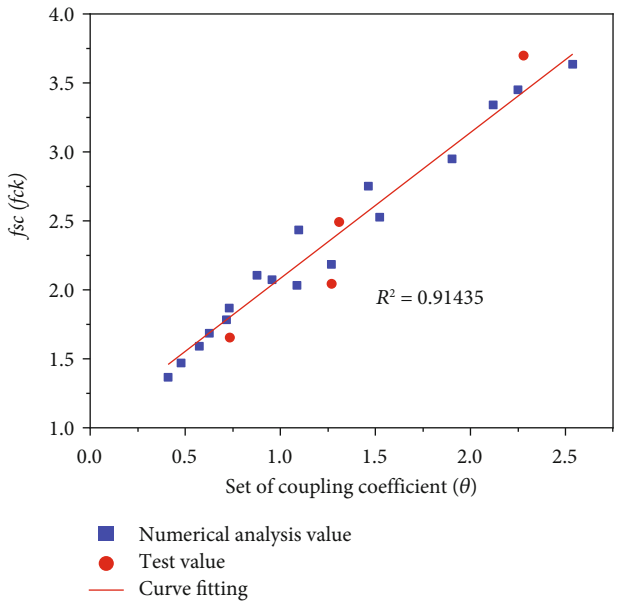

Figure 12: Relation between f_{sc}/f_{ck} and θ.

When $x \le 1$, $\varepsilon_{cc} = \varepsilon_c(1 + k_2(f_{rp}/\gamma_c f_c'))\,\varepsilon_c = 0.002$.

When $x > 1$, and $D/t = 50$, ε_{cc} is 0.0027, $D/t = 30$, and ε_{cc} is 0.0023, when $D/t < 30$, ε_{cc} equal to 0.0021. The diameter to thickness ratio can be calculated as a linear difference when the value between 30 and 50.

4.3. Modeling Parameters. Abaqus, a finite element software, is used to establish the analysis model, and 3D 8-node linear with reduced integration (C3D8R) is used to simulate both aluminum alloy tube and filled concrete (Figure 9). Surface-surface contact is used to define the interaction between aluminum tube and concrete. The hard contact model and isotropic Coulomb friction model were used to simulate along with the normal and tangential directions, respectively. Because aluminum tube and concrete are loaded at the same time, there is little or no sliding between aluminum tube and concrete; so, the friction coefficient has little influence on the structural performance of aluminum tube concrete column. Referring to the existing test results [16] and considering that the surface of aluminum tube is smoother than that of steel tube, the μ value equals to 0.4. The setting of boundary conditions is the same as the experiment. At the same time, considering astringency and calculation accuracy, the expansion angle is 30°, eccentricity is 0.1, the biaxial and uniaxial initial yield strength ratio f_{b0}/f_{c0} is 1.16, the ratio K of the second stress invariant in the tension-compression meridian plane is 0.667, and the viscosity parameter is 0.0005.

4.4. Finite Element Model Validation. Nephogram of finite element calculation is shown in Figure 10. Finite element simulation is calculated under ideal conditions, without considering the impact of test errors such as end effect and concrete coarse aggregate subsidence. The results show that the concrete in the column expands laterally. The finite element calculation curve is shown in Figure 11, and the calculation results of bearing capacity are shown in Table 7.

The finite element model proposed in this paper fits well with the test curve. The plastic section of the test curve is small because the compressive strength of the core concrete decreases continuously due to the degradation of constraints due to the crack generated after the peak point of aluminum alloy. The software calculation is different from the test results in the descending stage due to the limited of finite element software cannot simulate the aluminum alloy cracking and the internal concrete crushing. The ratio of peak bearing capacity between test results and finite element calculation results is between 0.956 and 1.019, and the error is less than 5%. The finite element calculation results can well predict the ultimate bearing capacity of specimens and the variation trend of stress-strain curves of specimens, which can be used to study the axial compression performance and bearing capacity of 7A04 aluminum alloy tube concrete, and also provide a theoretical basis for the subsequent simulation.

5. Calculation of Axial Bearing Capacity

At present, most of the bearing capacity calculation formulas of aluminum alloy tubular concrete columns are modified based on concrete-filled steel tube columns. For high-strength concrete-filled steel tubular columns, the strength and ductility of core concrete can be greatly improved due to the strong restraint of steel tube on concrete. It is found that there is no obvious plastic stage or small plastic stage in the axial compression process of 7A04 aluminum alloy tube concrete, but the strength drops rapidly after the peak point. This indicates that the concrete fragments form concentrated transverse damage to the aluminum tube, resulting in the rapid degradation of the transverse constraint on concrete. Therefore, it is necessary to explore the bearing capacity calculation method of composite column of aluminum tube concrete. In this paper, 17 groups of 7A04 aluminum alloy tube concrete short columns with different parameters are simulated by using the finite element model proposed in the fourth section. The diameter-thickness ratio is 33-80, the concrete strength is C30-C70, and the yield strength of the aluminum tube is 420 MPa.

The axial compression capacity of each column is divided by the total area of the section to obtain the composite strength of the specimen section (f_{sc}). The ratio (f_{sc}/f_{ck}) of the composite strength of the specimen section (f_{sc}) to

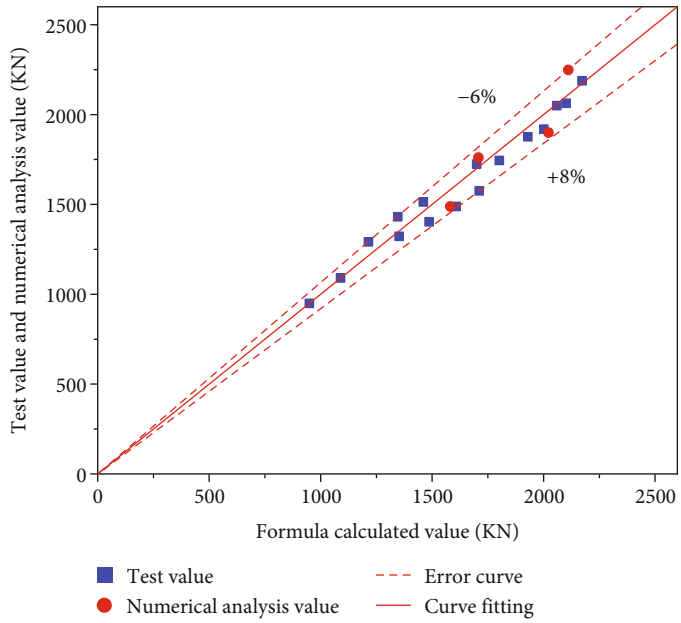

Figure 13: Comparison of the bearing capacity calculated by the formula with the experimental or simulated bearing capacity.

concrete axial compression strength (f_{ck}) is taken as longitudinal axis, and the constraint effect coefficient θ is taken as transverse axis. Linear regression analysis of the test and simulation results of 21 groups was performed, and the results are shown in Figure 12.

It is found that the ratio of the composite strength of the specimen section (f_{sc}) to axial compression strength (f_{ck}) of concrete has a linear relationship with the confinement coefficient (θ). Accordingly, the bearing capacity of the specimen can be expressed as follows as the fitting formula of the ratio of the composite strength of the specimen section to the axial compression strength of concrete and the confinement coefficient of the specimen.

$$f_{sc} = (1.11079\theta + 0.98244) f_{ck}. \tag{10}$$

The bearing capacity of 7A04 aluminum alloy tubular concrete short column can be calculated by the following formula, according to the "Unified Theory" of the calculation of the bearing capacity of the concrete filled steel tube short column.

$$N_{sc} = f_{sc} A_{sc}, \tag{11}$$

where N_{sc} is the bearing capacity of the specimen, and A_{sc} is the cross-section area of the specimen.

As shown in Figure 13, the comparison error between the calculation formula of the bearing capacity proposed in this paper and the simulated value is in the range of -6% ~8%, and the comparison error with the experimental value is in the range of -6% ~6%. The bearing capacity calculation formula of the 7A04 aluminum tube concrete column suggested takes into account the interaction between aluminum tube and concrete, which can accurately predict the bearing capacity of such aluminum tube concrete members.

6. Conclusion

The following conclusions can be drawn based on a series of tests conducted on 7A04 high strength aluminum alloy tube filled concrete short columns:

(1) The failure modes of specimens are mainly middle swelling and shear failure. The load-strain curve of specimens is divided into four stages, and each stage is analyzed. Due to the poor plasticity of 7A04, there is no obvious plastic stage in the load-strain curve of the specimen, and there are different degrees of decrease after the peak point

(2) In the test process, 7A04 high strength aluminum alloy tube concrete short column shows the strength comparable to that of high strength steel tube filled concrete. However, the ductility of the specimen decreases slightly with the improvement of the strength grade of the filled concrete. In order to make the specimens show good ductility to meet the needs of practical engineering, the tube thickness of aluminum tube can be appropriately increased while the strength of the filled concrete can be reduced

(3) The finite element model of 7A04 high strength aluminum alloy tube concrete short column is proposed considering the compound action between aluminum alloy tube and concrete. This constitutive curve accurately reflects the mechanical characteristics of the specimen under axial compression and fits well with the test curve. Further research is needed to better fit the descending section of the curve

(4) A formula for calculating the bearing capacity of the 7A04 aluminum alloy tube concrete short column is proposed. The formula can predict the strength of the 7A04 aluminum alloy tube concrete short column well by calculation. Due to the limited number of specimens in this test, the complex mechanical characteristics between high-strength aluminum tube and core concrete still need to be further explored

Data Availability

The data are generated from experiments and can be available from the corresponding author upon request. Their financial support is highly appreciated.

Conflicts of Interest

The authors declare that there are no conflicts of interest regarding the publication of this paper.

Acknowledgments

This study was supported by the Natural Science Foundation of Xinjiang Uygur Autonomous Region (2019D01C028).

References

[1] E. Ellobody, B. Young, and D. Lam, "Behaviour of normal and high strength concrete-filled compact steel tube circular stub columns," *Journal of Constructional Steel Research*, vol. 62, no. 7, pp. 706–715, 2006.

[2] R. Wang, L. H. Han, J. G. Nie, and X. L. Zhao, "Flexural performance of rectangular CFST members," *Thin-Walled Structures*, vol. 79, pp. 154–165, 2014.

[3] R. Yadav, B. Chen, and Y. Hui Hui, "Numerical study on the seismic behavior of CFST columns," in *11th Pacific Structural Steel Conference*, vol. 2931, pp. 360–369, Shanghai, China, 2016.

[4] L. H. Han and Y. F. An, "Performance of concrete-encased CFST stub columns under axial compression," *Journal of Constructional Steel Research*, vol. 93, pp. 62–76, 2014.

[5] Z. SHEN, X. GUO, and Y. LI, "State-of-the-arts of research on aluminum alloy structures," *Journal of Building Structures*, vol. 28, no. 6, pp. 100–109, 2007.

[6] L. H. Han, W. Li, and R. Bjorhovde, "Developments and advanced applications of concrete-filled steel tubular (CFST) structures: members," *Journal of Constructional Steel Research*, vol. 100, pp. 211–228, 2014.

[7] M. Szumigała and Ł. Polus, "Applications of aluminium and concrete composite structures," *Procedia Engineering*, vol. 108, pp. 544–549, 2015.

[8] Y. X. Hua, L. H. Han, Q. L. Wang, and C. Hou, "Behaviour of square CFST beam-columns under combined sustained load and corrosion: experiments," *Thin-Walled Structures*, vol. 136, pp. 353–366, 2019.

[9] C. Hou, L. H. Han, and X. L. Zhao, "Full-range analysis on square CFST stub columns and beams under loading and chloride corrosion," *Thin-Walled Structures*, vol. 68, pp. 50–64, 2013.

[10] R. Narayanan, *Aluminium structures*, London and New York, Elsevier Applied Science, 1987.

[11] ECCS, *European Reconmmendations for Aluminmum alloy structures*, First edn editionFirst edn edition, , 1978.

[12] D. A. S. SK and K. A. U. F. M. A. N. JG, "Aluminum alloys for bridgesand bridge decks," in *Aluminum Alloys for Transportation, Packaging, Aerospace, and Other Application*, D. A. S. SK and Y. I. N. Weimin, Eds., pp. 61–72, The Minerals, Metals & Materials Society, 2007.

[13] S. Ayata and W. Ensinger, "Ion beam sputter coating in combination with sol-gel dip coating of Al alloy tube inner walls for corrosion and biological protection," *Surface and Coatings Technology*, vol. 340, pp. 121–125, 2018.

[14] S. Hu, L. Liu, Y. Cui, Y. Li, and F. Wang, "Influence of hydrostatic pressure on the corrosion behavior of 90/10 copper-nickel alloy tube under alternating dry and wet condition," *Corrosion Science*, vol. 146, pp. 202–212, 2019.

[15] National standards of the People's Republic of China GB 50429-2007, *Code for design of aluminium structures*, Beijing: Standards Press of China, 2007.

[16] W. Zeng Xiang, H. J.-s. Wan-bo, and H. Tao, "Study on axial compression bearing capacity of circular aluminum alloy tube concrete short columns," *Engineering mechanics*, vol. 38, no. 2, pp. 52–60, 2021.

[17] F. Zhou and B. Young, "Tests of concrete-filled aluminum stub columns," *Thin-Walled Structures*, vol. 46, no. 6, pp. 573–583, 2008.

[18] F. Zhou and B. Young, "Numerical analysis and design of concrete-filled aluminum circular hollow section columns," *Thin-Walled Structures*, vol. 50, no. 1, 2012.

[19] F.-C. Wang, H.-Y. Zhao, and L.-H. Han, "Analytical behavior of concrete-filled aluminum tubular stub columns under axial compression," *Thin-Walled Structures*, vol. 140, pp. 21–30, 2019.

[20] L. Yue Qing and D. J. Laurie Kennedy, "The flexural behaviour of concrete-filled hollow structural sections," *Canadian Journal of Civil Engineering*, vol. 21, no. 1, pp. 111–130, 1994.

[21] R. Feng, Y. Chen, and W. Gong, "Flexural behaviour of concrete-filled aluminium alloy thin-walled SHS and RHS tubes," *Engineering Structures*, vol. 137, pp. 33–49, 2017.

[22] Y. Chen, R. Feng, and J. Xu, "Flexural behaviour of CFRP strengthened concrete-filled aluminium alloy CHS tubes," *Construction and Building Materials*, vol. 142, pp. 295–319, 2017.

[23] W. Zhang, X. K. Xiao, and G. Wei, "Constitutive relation and fracture model of 7A04 aluminum alloy," *Explosion and shock waves*, vol. 31, no. 1, pp. 81–87, 2011.

[24] Y. Q. Wang, Z. X. Wang, X. G. Hu, J. K. Han, and H. J. Xing, "Experimental study and parametric analysis on the stability behavior of 7A04 high-strength aluminum alloy angle columns under axial compression," *Thin-Walled Structures*, vol. 108, pp. 305–320, 2016.

[25] D. Chao Fang, X. Kui, and X. Lin, "Characterization of 7A04 aluminum alloy corrosion under atmosphere with chloride ions using electrochemical techniques," *Rare Metal Materials and Engineering*, vol. 40, pp. 275–279, 2011.

[26] Z. Tao, L.-H. Han, and D.-Y. Wang, "Strength and ductility of stiffened thin-walled hollow steel structural stub columns filled with concrete," *Thin-Walled Structures*, vol. 46, no. 10, pp. 1113–1128, 2008.

[27] P. K. Gupta, S. M. Sarda, and M. S. Kumar, "Experimental and computational study of concrete filled steel tubular columns under axial loads," *Journal of Constructional Steel Research*, vol. 63, no. 2, pp. 182–193, 2007.

[28] K. Sakino and H. Hayashi, "Behavior of concrete fifilled steel tubular stub columns under concentric loading," in *Proceedings of the 3rd International Conference on Steel-Concrete Composite Structures*, pp. 25–30, Fukuoka, Japan, 1991.

[29] N. J. Gardner and R. Jacobson, "Structural behaviour of concrete fifilled steel tubes," *ACI Journal Proceedings*, vol. 64, no. 7, 1967.

[30] J. Y. R. Liew and D. X. Xiong, "Experimental investigation on tubular columns infifilled with ultra-high strength concrete," in *Proceedings of the 13th International Symposium on Tubular Structures*, pp. 637–645, Hong Kong, China, 2010.

[31] W. Ramberg and W. R. Osgood, *Description of stress-strain curves by three parameters*, Washing-ton DC: NACATN-902, 1943.

[32] S. P. Schneider, "Axially loaded concrete-filled steel tubes," *Journal of Structural Engineering*, vol. 124, no. 10, pp. 1125–1138, 1998.

[33] P. V. Ishvarbhai, L. Q. Quan, and N. S. Hadi Muhammad, "Numerical analysis of circular double-skin concrete-filled stainless steel tubular short columns under axial loading," *Structure*, vol. 24, 2018.

[34] V. I. Patel, Q. Q. Liang, and M. N. S. Hadi, "Numerical simulations of circular high strength concrete-filled aluminum tubular short columns incorporating new concrete confinement model," *Thin-Walled Structures*, vol. 147, p. 106492, 2020.